Effects of Using High Resolution Satellite-based Inundation Time Series to Estimate Methane Fluxes from Forested Wetlands

Kelly L. Hondula[1], Ben DeVries[2], C. Nathan Jones[3], and Margaret A. Palmer[1]

[1]National Socio-Environmental Synthesis Center, University of Maryland, MD, USA.
[2]Department of Geography, Environment and Geomatics, University of Guelph, Ontario, Canada. [3]Department of Biological Sciences, University of Alabama, AL, USA.

Corresponding author: Kelly Hondula (kellyhondula@gmail.com)

Key Points:

- Variable inundation extent in forested wetlands has large implications for calculating methane emissions.
- Surface water maps based on 30m imagery likely exclude wetlands that contribute a majority of methane emissions from forested landscapes.
- High resolution optical imagery underestimates surface water extent in forested wetland landscapes during periods of high canopy cover.

Abstract

A major source of uncertainty in the global methane budget arises from quantifying the area of wetlands and other inland waters. This study addresses how the dynamics of surface water extent in forested wetlands affect the calculation of methane emissions. We used fine resolution satellite imagery acquired at sub-weekly intervals together with a semi-empirical methane emissions model to estimate daily surface water extent and diffusive methane fluxes for a low-relief wetland-rich watershed. Comparisons of surface water model predictions to field measurements showed agreement with the magnitude of changes in water extent, including for wetlands with surface area less than 1,000 m^2. Results of methane emission models showed that wetlands smaller than 1 hectare (10,000 m^2) were responsible for a majority of emissions, and that considering dynamic inundation of forested wetlands resulted in 49–62% lower emission totals compared to models using a single estimate for each wetland's size.

Plain Language Summary

Wetlands and small ponds are hotspots for greenhouse gas emissions, especially methane. Quantifying how much, though, depends on accurately mapping each of those water bodies. Whereas most medium and large lakes are visible to satellites, smaller bodies are generally missing from the best maps and flooded areas in forests are overlooked. Additionally, many of these systems change in size depending on the current season and rainfall patterns. We use several hundred high resolution satellite images collected over the same forested region over the course of one year to estimate how much water bodies changed in size, and the subsequent effect that has on methane emissions from this area. We found that wetlands only visible in high resolution imagery were responsible for most of the total methane emissions, and that accounting for changing wetland size throughout the year halved the estimated emissions.

1 Introduction

Global change is affecting the quantity, quality, and timing of material fluxes through ecosystems with consequences for the fate and transformation of carbon. Inland waters are now recognized as fundamental to understanding the global carbon (C) cycle (Cole et al., 2007; Raymond et al., 2013; Tranvik et al., 2009) yet our ability to characterize C fluxes and their drivers at landscape and regional scales remains limited by available data on surface water extent (SWE) and dynamics—particularly for forested wetlands, very small water bodies (e.g. ponds), and areas with temporally varying inundation. Collectively, these limitations represent a major shortcoming in our ability to account for methane emission sources, and at least one third of all uncertainty in the global methane budget (Melton et al., 2013; Saunois et al., 2020).

Methane emissions for lakes, ponds, reservoirs, streams, and rivers have been calculated by upscaling the best available data on flux rates and the areal extent of those waters by category (Saunois et al., 2020). However, for wetlands, a combination of land cover maps, remote sensing data, and simulated hydrologic fluxes are used to calculate temporally varying methane producing areas as inputs to process-based biogeochemical models (Poulter et al., 2017; Wania et al., 2012). Both approaches suffer from uncertainties associated with spatial and temporal variation in inundation extent which is highly relevant for resolving sources and sinks of methane at global scales. This wetland extent problem contributes substantial uncertainty in

methane budgets and limits our ability to identify drivers of recent increases in atmospheric concentrations (Thornton et al., 2016).

Upscaling empirical data on gas flux rates to quantify freshwater methane emissions is fraught with biases, including inadequate representation of underlying drivers (DelSontro et al., 2018; Seekell et al., 2014) and lack of consideration of seasonal events such as ice-out or non-growing season emissions (Treat et al., 2018). Despite advances in remote sensing of aquatic systems, identifying small water bodies remains a challenge because they are often optically complex, obscured by vegetation, or below the resolvable size of satellite sensors (Allen & Pavelsky, 2018; Kuhn et al., 2019). The resulting omission of forested wetlands, small water bodies, and inundation dynamics in land cover and surface water data sets is broadly recognized (DeVries et al., 2017; Lang et al., 2020), but its implications for methane emissions accounting is unresolved (Poulter et al., 2017; Thornton et al., 2016). This is despite recognition that headwaters and small water bodies play disproportionate roles in ecosystem processes (Hanson et al., 2007; Holgerson & Raymond, 2016; Lowe & Likens, 2005) and may comprise the largest proportion of freshwater area (Bishop et al., 2008; Downing et al., 2006).

The ability to monitor and detect surface water at higher spatial and temporal resolution is advancing through new technologies including sub-pixel methods (DeVries et al., 2017), fusion with hydrologic models (Evenson, Golden, et al., 2018), satellite constellations (Claverie et al., 2018; Cooley et al., 2019), and applications of machine learning (Jia et al., 2018; Lang et al., 2020; Lee et al., 2019). However, most remote sensing applications for freshwater bodies remain focused on relatively large or unvegetated systems (Griffin et al., 2018; Kuhn et al., 2019; Pekel et al., 2016) by excluding pixels influenced by fractional coverage of soil and vegetation (Ji et al., 2009). Using such methods is warranted to avoid classification errors associated with spectral unmixing (Halabisky et al., 2016), but it can also result in large uncertainties for C fluxes at regional or global scales (Melton et al., 2013; Thornton et al., 2016; Treat et al., 2018) due to substantial underrepresentation of SWE (DeVries et al., 2017). Previous studies have explored inter-annual variability in wetland extent (Huang et al., 2014; Lang et al., 2020; Yeo et al., 2019) but investigation of intra-annual dynamics has generally been limited by availability of cloud-free leaf-off imagery. Further, most investigations have not characterized inundation patterns for individual wetlands (Vanderhoof et al., 2018) or used sub-pixel estimation techniques (DeVries et al., 2017; Yeo et al., 2019) to account for the preponderance of small water bodies that result in mixed spectral signatures for pixels in 30 m resolution imagery.

Discrepancies between top-down and bottom-up emissions tend to be largest from forested areas (Melton et al., 2013). Recent investigations into these discrepencies have uncovered new sources and emission pathways from trees (Pangala et al., 2017). Further, in tropical regions, wetland emission models underestimate emissions compared to observations with the largest discrepancy in years with significant wetland flooding (Parker et al., 2018). Because surface water maps exclude most under-canopy inundation, evasion from these inundated regions may also play an important role in explaining emissions from seasonally dynamic temperate forested areas that are not reproduced in existing wetland models.

This study was designed to fill gaps in our understanding of how forested wetland size and temporal variation in inundation influence watershed-scale estimates of methane emissions. We combine elements from both the wetland and inland water calculation approaches described

above to estimate one year of diffusive methane emissions from forested wetlands across a 347 km^2 mid-Atlantic Coastal Plain watershed. We use fine resolution frequent-repeat remote sensing imagery to estimate daily SWE at the wetland scale as input to field-validated semi-empirical models for calcuating methane emissions. As in other studies, we assume SWE is a proxy for methane producing area. Results demonstrate that i) excluding inundation variability increased modeled methane emission totals by 66–105%, but ii) excluding small water bodies (< 1,000 m^2) reduced inundation estimates and subsequent emissions by 30% and 38–51%.

2 Methodology

2.1 Study area

Our study site, the 347 km^2 Greensboro watershed, is on the Delmarva Peninsula (Maryland, USA), a low-gradient coastal plain landscape defined by poorly drained soils and the persistence of small depressional forested wetlands surrounded by extensive ditch-drained agricultural land (Figure 1; Jones et al., 2018). Known as Delmarva Bays, these wetlands range in size from small closed canopy wetlands (<0.5 ha; similar to vernal pools in the northeast) to large open canopy wetlands (>5 ha; similar to Carolina Bays) (Phillips & Shedlock, 1993). Typically they dry seasonally, having maximum inundation during the winter and decreasing water levels through the spring and summer due to evapotranspiration and agricultural groundwater withdrawal (Lee et al., 2020).

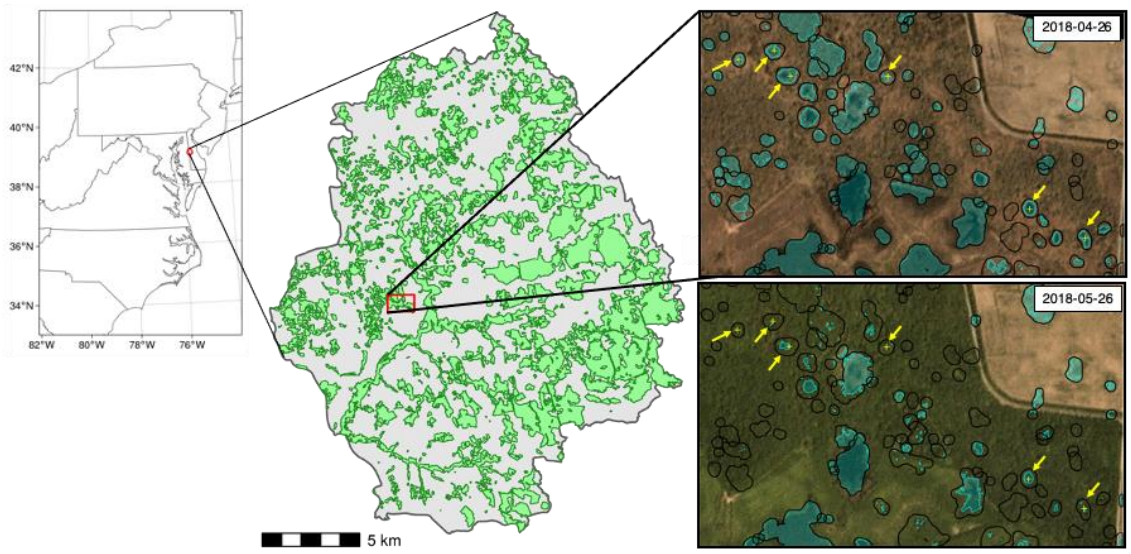

Figure 1. Study area showing location of the Greensboro watershed and forested wetlands. Wetland boundaries, monitoring locations, and surface water classification model predictions for 2 images are shown over corresponding color-corrected PlanetScope Visual Ortho Scenes (Planet, 2018).

Draining to the Chesapeake Bay via the Choptank River, this watershed has been the focal point for extensive research (e.g., Ator & Denver, 2012). Land cover is mainly cultivated crops (50.5%), woody wetlands (31.5%), and deciduous forest 7.7% (Jin et al., 2019). We define wetlands using a previously developed dataset of topographic depressions (Vanderhoof & Lang,

2017) that were derived using the Stochastic Depression Analysis Tool (Lindsay, 2016; Wu et al., 2014) and filtered using a minimum size of 50 m^2 and SWE classified from April 2015 Worldview 3 imagery (Vanderhoof et al., 2018). Polygons generally co-occur with features in the National Wetlands Inventory (NWI) but they are more numerous, cover less total area, and are more spatially aligned with SWE. We subset this dataset to only those within woody wetlands land cover using the 2016 National Land Cover Database (NLCD; Jin et al., 2019). This approach resulted in 5,118 forested wetland depressions (46% of those in the watershed), which we refer to as focal wetlands.

2.2 Remote sensing for surface water classification

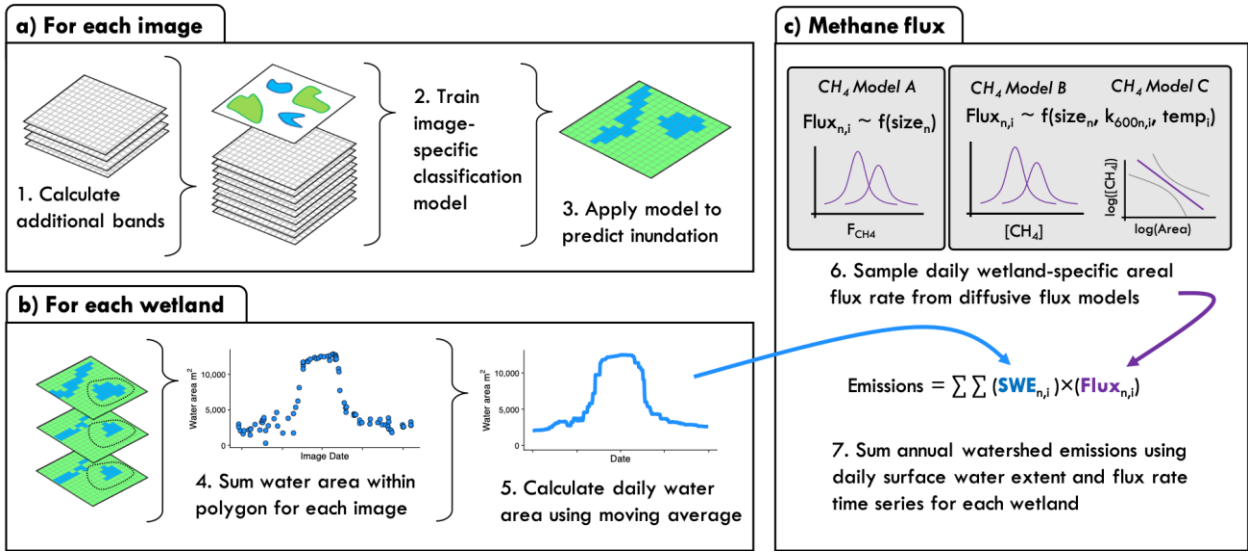

Figure 2. Image classification and emissions model workflow. **a)** Image-specific supervised classification models developed using original 4 bands (R, G, B, NIR) and derived indices NDVI, NDWI, saturation, chroma, and luminesce; **b)** Daily surface water time series derived for each focal wetland from predicted surface water area within each polygon boundary across all images; **c)** Methane emissions for each wetland (n) on day (i) derived using semi-empirical models to produce annual estimates of basin-wide emissions.

Daily time series of SWE for each focal wetland were calculated using 3 m resolution PlanetScope imagery (Figure 2; Text S1; Planet, 2018). We downloaded 421 PlanetScope 4-band images that overlapped the study watershed and had less than 1% cloud cover. These were taken across 98 days in the 2018 water year, during which wetland surface water levels were monitored in the field. All images were Surface Reflectance products, which were atmospherically corrected using the 6SV2.1 radiative transfer model (Planet, 2018; Vermote et al., 1997). Images were masked to exclude low quality pixels indicated by the unusable data mask provided with each image. Then, we calculated a suite of spectral indices from the four bands in each image, including NDWI (McFeeters, 1996), NDVI (Tucker, 1979), saturation, luminescence, and chroma (Zeileis et al., 2019), resulting in 9 variables for each pixel.

Training data for surface water and non-water classes were based on the NWI, the 2016 NLCD, and the wetland depressions dataset developed by (Vanderhoof & Lang, 2017). We

defined surface water as Freshwater Pond (n = 655) and Lake (n = 1) classes in NWI, which are classified in NWI as permanently (99%) or semi-permanently (1%) flooded. We defined non-water areas using NLCD forest and forested wetland classes minus pixels falling within 10m of any NWI polygons or topographic depressions. For each image, pixel values for the 9 bands in the training regions were extracted and a sample was used to train a random forest model that was then applied to the image.

For each classified image, we extracted pixel values within a 10m buffer around each focal wetland to calculate the predicted inundation area (Figure 2b). We used the buffer to account for the 10m geolocation uncertainty in the optical data (Planet, 2018), as well as potential expansion of inundation beyond topographic spill points, as is common in this landscape (Jones et al., 2018). Average time between usable images of each focal wetland was 6 days, resulting in a time series with 50-102 predictions across the year for each focal wetland. Average maximum time between consecutive usable images was 32 days but ranged up to 74 days. We converted the irregularly spaced predictions into a daily time series for each focal wetland using a 50-day rolling median. Time series with gaps longer than 50 days (1%) were excluded from total inundated surface area.

2.3 Field measurements

For comparison to areal extent of surface water estimated from remote sensing imagery, SWE was measured in the field at 6 wetlands in the study region (Figure 1). Water level was monitored in surface water wells at each wetland center using pressure transducers (Onset HOBO U20L level loggers) recording every 15 minutes. We calculated a daily time series of inundation extent for each wetland using binary classification of a 1m LiDAR-based digital elevation model (Lang et al., 2012) using mean daily water level with a raster-based approach similar to Jones et al., (2018). Estimates were validated using monthly observations of water extent along a fixed transect at each wetland as well as surveys around the perimeter of maximum observed inundation extent in mid-March 2018.

2.4 Methane emissions model

Daily diffusive methane emissions were calculated using wetland-specific flux rates and predicted daily SWE time series from the random forest classification models (Figure 2c). We developed three models (hereafter referred to as models A, B and C) using variations of a semi-empirical flux rate equation based on the synthesized global dataset of methane concentrations described by Holgerson and Raymond (2016) and validated with field measurements at 6 wetlands in the study area (Text S2). Model A predicted daily flux rates by sampling the lognormal distribution of the appropriate logarithmic size class for each wetland. For models B and C, daily flux rates for each wetland [n] were determined using Equation 1 with daily air temperature and atmospheric pressure from a nearby weather station to calculate gas exchange rates and equilibration concentrations of 1.85 ppm atmospheric methane for each day [i] (Winslow et al., 2016). $C_{aq[n]}$ is a time-invariant methane concentration for each wetland [n]

based on its size. Gas exchange rates were calculated using daily temperature values and the size-class specific k_{600} values described in Holgerson and Raymond (2016).

Equation 1: $$Flux_{n,i} = k_{n,i} \times \left(C_{aq[n]} - C_{eq[i]}\right)$$

For model B, $C_{aq}[n]$ was randomly sampled from a lognormal distribution based on the size class of each focal wetland's original area, and for model C, $C_{aq}[n]$ was predicted from the area-concentration regression model. Because forested wetlands are a high outlier for methane on the relationship between water body size and methane concentration reported by Holgerson and Raymond (2016), our calculated emissions are likely a conservative estimate. We estimated flux rate uncertainty using Monte Carlo resampling to generate a distribution of emission estimates for each wetland by running each model 1,000 times. Cumulative annual emissions across all wetlands were calculated using Equation 2, where SWE[n,i] is the SWE of depression [n] on day [i] calculated from the classification model time series.

Equation 2: $$Total\ Emissions = \sum\sum Flux_{n,i} \times SWE_{n,i}$$

We evaluated the effects of different model assumptions by calculating total annual methane emissions under each model with and without changes in SWE, based on the original area of each focal wetland. Models accounting for changes in SWE we call dynamic area models; models not accounting for these we call static area models.

3 Results

3.1 Magnitude and variability of predicted SWE

Total predicted SWE within focal forested wetlands across the watershed ranged from a low of 1.3 km^2 in late July to 6.2 km^2 in early April, with an average of 3.75 km^2. This area was an order of magnitude higher than maximum extent reported for the watershed in the global surface water area database (0.70 km^2; (Pekel et al., 2016)) and represents 2.5-5.7% of the entire watershed area, 50-113% of the area of topographic depressions, and 10-23% of the total area of NWI palustrine wetlands (U. S. Fish and Wildlife Service, 2019).

3.2 Classification model performance

Classification models were sufficiently able to discriminate between water and non-water areas. Comparisons between field-based and satellite-based inundation time series show that our modeling approach was able to quantify the magnitude of seasonal changes in SWE for individual wetlands, even for those smaller than 1,000 m^2. For the field-monitored wetlands, the maximum predicted extent and range from classification models were significantly related to observed values ($\rho = 0.91$, $\rho = 0.83$, respectively; $\alpha = 0.05$). However, the models consistently underpredicted May and June 2018 SWEs and overestimated November 2017 SWE (Figure 3). Monthly averaged residuals between field and satellite-based wetland areas were largest during these two periods (Figure 3b), but only in autumn 2017 was model accuracy also low (Figure

3a). The Nash-Sutcliffe (NSC) criteria to evaluate model efficiency indicated poor fit (NSE <0.5) between the daily simulated and observed water extents.

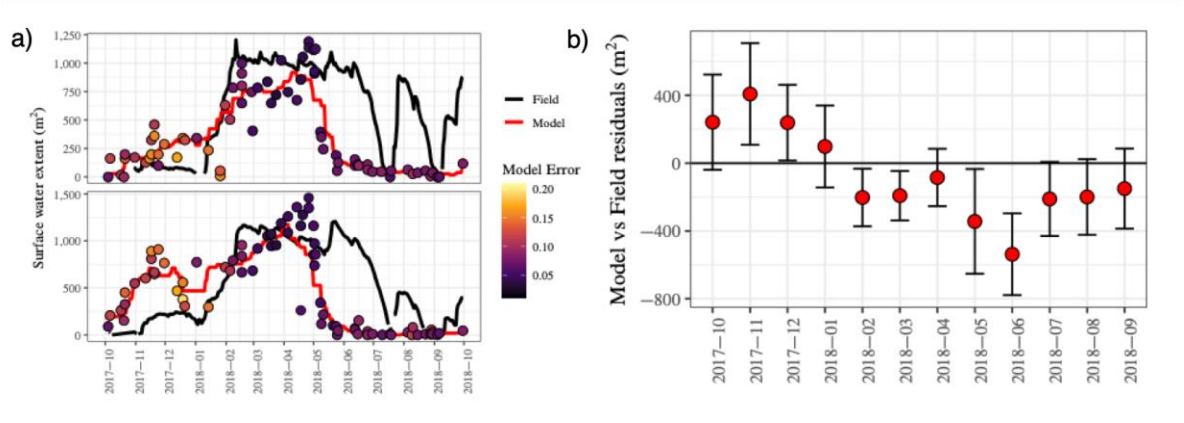

Figure 3. Comparison between inundation time series developed from field monitoring and satellite data. **a)** Inundation time series from two wetlands comparing field data and predictions from image-based classification models, along with estimates from individual images (points) shaded by model error rate. **b)** Average monthly residuals (± sd) between model predictions of SWE from image classification and field data for all observations across the 6 wetlands with field water level data.

3.3 Methane emission totals under different model assumptions

Calculating watershed methane emissions using a time series approach to quantify variation in surface water coverage resulted in total estimated annual emissions 49-62% lower than when static wetland sizes were used (Figure 4a). Using the concentration-area regression flux model (C) resulted in higher emission totals than either the size category flux (A) or size category concentration (B) models, but in all three cases the difference between the dynamic and static models was substantially greater than variability associated with methane flux rate uncertainty. We also observed that small wetlands (< 1 ha) were responsible for a considerable proportion of modeled emissions. Although the static area models overestimated emissions for any given minimum wetland size threshold, they are only overestimates compared to the best estimate of total emissions if wetlands smaller than 1,000 m^2 are included. Excluding these

resulted in an underestimate of total emissions by at least 10% and excluding wetlands smaller than 0.01 km^2 underestimated emissions by at least 75% (Figure 4b).

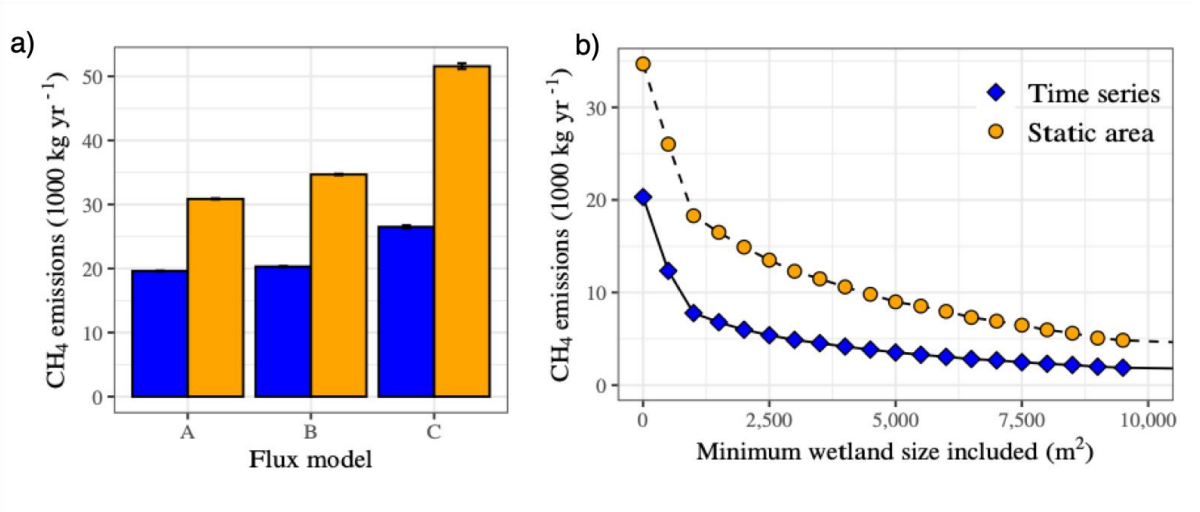

Figure 4. Total annual diffusive methane emissions for focal wetlands calculated using different model assumptions. **a)** Total emissions for time-varying (blue) vs. static (orange) estimates of SWE using the 3 semi-empirical diffusive flux models described in Section 2.4. Error bars represent 5% and 95% quantiles from 1,000 model iterations. **b)** Total emissions for time-varying vs. static SWE with different minimum wetland size thresholds.

4 Discussion

We demonstrate that accounting for inundation and variable SWE in forested wetlands significantly influences calculations of diffusive methane emissions from a low-relief wetland-rich watershed. Specifically, we show that: i) previous limitations in quantifying SWE at the global scale will typically result in underestimates of methane emissions from forested wetlands; ii) as spatial resolution of wetland map products improve, accurate estimates of emissions will require improved quantification of intra-annual surface water dynamics; and iii) while fine-resolution frequent-revisit satellite imagery can help address these gaps, our ability to detect and monitor sub-canopy inundation during the late growing season is still limited. Below we discuss modeling inundation dynamics in forested wetlands and implications for the global methane budget in more detail.

4.1 Modeling inundation dynamics of forested wetlands using high resolution satellite data

This study shows that it is possible to quantify intra-annual surface water dynamics in small forested wetlands (< 1,000 m^2) using optical satellite data that has both fine spatial and high temporal resolution. Although classification models were able to produce inundation time series with similar patterns to the field-based time series (Figure 3), they also had consistent

inaccuracies, demonstrating that optical imagery alone does not accurately represent the timing of surface water dynamics in forested wetlands, especially after leaf-out.

In fall 2017, satellite-derived SWE was overestimated compared to our field measurements. We hypothesize this is attributable to unreliable classification of "permanent" water features in the NWI, i.e. many of these water bodies are actually seasonal. Few alternatives exist for accurate training data at spatial resolutions necessary to identify the smallest water bodies, and quantitative information on hydrologic regimes is even less common. Even though the NWI is very detailed and thematically rich, it has known inaccuracies in the Delmarva region (Fenstermacher et al., 2014). Whereas variability in radiometry between Planet images required using image-specific models in this study, data from a more consistent sensor constellation (e.g., Claverie et al., 2018) could potentially be used with a more universal classification model based only on training data from time points and locations where inundation status is known with more certainty. However, seasonal and event-driven patterns of suspended sediment, chlorophyll *a*, and dissolved carbon (Hosen et al., 2018) could affect the optical properties of these water bodies in ways that would impact model reliability .

In 2018, underestimates of surface water area in May and June coincided with the timing of canopy leaf-out. We hypothesize that underestimates are attributable to the lag between structural change in the forest canopy and the subsequent regional contraction of SWE (Figure 3a; Fisher et al., 2010; Lee et al., 2019). Canopy cover developing above areas that remain flooded, such as on the periphery of wetland depressions, obscures surface water in optical imagery. Improved methods for inundation detection under forest canopies may be possible using synthetic aperture radar (SAR; Lang et al., 2008; Lang & Kasischke, 2008), combinations of optical and lidar intensity data (Lang et al 2020), or improved integration with field monitoring and hydrologic models that account for upland topographic depressions (Evenson et al., 2018). While long-wavelength SAR sensors have been shown to be sensitive to under-canopy inundation in forested wetlands (Arnesen et al., 2013; Xaypraseuth et al., 2015), these data are not yet publicly available. Future satellite missions like the NASA-ISRO SAR (NISAR) mission, planned for launch in 2022, will provide repeat long-wavelength SAR imagery and thus play an important role in improving estimates of surface water dynamics in forested wetlands.

4.2 Implications for upscaling methane emissions

As field studies continue to document high concentrations of methane in aquatic ecosystems previously overlooked as sources of emissions (Bastviken et al., 2011; Stanley et al., 2015), inventory-based emission estimates of global freshwater methane fluxes have become larger, more uncertain, and more at odds with top-down estimates in the global methane budget (Saunois et al., 2020). Our results show that for a given set of water bodies, inventory-based emission estimates can be too high in areas where inundation extent fluctuates on a seasonal basis. However, non-permanent water bodies are also likely to be underrepresented in surface water products or mis-classified in existing landcover products due to their small size and/or obscuration by forest cover. Because the highest resolution global surface water dataset is based on non-mixed 30 m pixels (Pekel et al., 2016), water bodies < ~1,000 m^2 will be absent. At this

threshold, the opposing effects of inundation dynamics and missing hidden/cryptic water bodies were of similar magnitude and resulted in a 10% underestimate of annual totals.

Understanding the source of methane is important for mitigation strategies and policies aimed at reducing carbon emissions from local to global scales. Traditional upscaling approaches for greenhouse gas emissions from freshwaters can be misleading for determining the dominant factors driving emissions (DelSontro et al., 2018). Our results suggest that for the Greensboro watershed, the water level drawdown in natural forested wetlands considerably reduces methane producing areas. Where forested wetlands are lost and replaced with wetlands without a similar hydroperiod, such as many wetland mitigation projects (e.g., created ponds) that result in a net increase in total surface area (Dahl, 2011), methane emissions are likely to be higher. Farm ponds and other small artificial water bodies have also been shown to have higher methane emissions on a per-area basis (Grinham et al., 2018; Ollivier et al., 2019), and a relatively constant water level only exacerbates this difference because natural wetlands have reduced SWE during the warmest months when methane production rates could be the highest. The ability to detect and monitor under-canopy inundation should improve with new space-borne longer wavelength synthetic aperture radar (Arnesen et al., 2013; Xaypraseuth et al., 2015); as these capabilities improve accurately quantifying ecosystem functions of forested wetlands will also require information at high temporal resolution. Future studies may leverage these improved technologies to better understand the role forested wetlands are playing in regional and global methane cycles by more accurately quantifying the hydrologic processes underyling methane flux to the atmosphere from inland waters.

Acknowledgments, Samples, and Data

Datasets used in this research are available in cited references: Holgerson and Raymond (2016), Vanderhoof and Lang (2017); Pekel et al. (2016); Jin et al (2019); USFWS (2019); and Planet (2017). Planet data are available through personal licenses to researchers for non-commercial purposes. Processing and analysis code is available online as https://github.com/khondula/ch4est. This work was supported by the National Socio-Environmental Synthesis Center under funding received from the National Science Foundation DBI-1639145.

References

Allen, G. H., & Pavelsky, T. M. (2018). Global extent of rivers and streams. *Science*, *361*(6402), 585–588. https://doi.org/10.1126/science.aat0636

Arnesen, A. S., Silva, T. S. F., Hess, L. L., Novo, E. M. L. M., Rudorff, C. M., Chapman, B. D., & McDonald, K. C. (2013). Monitoring flood extent in the lower Amazon River floodplain using ALOS/PALSAR ScanSAR images. *Remote Sensing of Environment*, *130*, 51–61. https://doi.org/10.1016/j.rse.2012.10.035

Ator, S. W., & Denver, J. M. (2012). Estimating Contributions of Nitrate and Herbicides From Groundwater to Headwater Streams, Northern Atlantic Coastal Plain, United States [1]: ESTIMATING CONTRIBUTIONS OF NITRATE AND HERBICIDES FROM GROUNDWATER TO HEADWATER STREAMS, NORTHERN ATLANTIC COASTAL PLAIN, UNITED STATES. *JAWRA Journal of the American Water Resources Association*, *48*(6), 1075–1090. https://doi.org/10.1111/j.1752-1688.2012.00672.x

Bastviken, D., Tranvik, L. J., Downing, J. A., Crill, P. M., & Enrich-Prast, A. (2011). Freshwater Methane Emissions Offset the Continental Carbon Sink. *Science*, *331*(6013), 50–50. https://doi.org/10.1126/science.1196808

Bishop, K., Buffam, I., Erlandsson, M., Fölster, J., Laudon, H., Seibert, J., & Temnerud, J. (2008). Aqua Incognita: The unknown headwaters. *Hydrological Processes*, *22*(8), 1239–1242. https://doi.org/10.1002/hyp.7049

Claverie, M., Ju, J., Masek, J. G., Dungan, J. L., Vermote, E. F., Roger, J.-C., Skakun, S. V., & Justice, C. (2018). The Harmonized Landsat and Sentinel-2 surface reflectance data set. *Remote Sensing of Environment*, *219*, 145–161. https://doi.org/10.1016/j.rse.2018.09.002

Cole, J. J., Prairie, Y. T., Caraco, N. F., McDowell, W. H., Tranvik, L. J., Striegl, R. G., Duarte, C. M., Kortelainen, P., Downing, J. A., Middelburg, J. J., & Melack, J. (2007). Plumbing the Global Carbon Cycle: Integrating

Inland Waters into the Terrestrial Carbon Budget. *Ecosystems*, *10*(1), 172–185. https://doi.org/10.1007/s10021-006-9013-8

Cooley, S. W., Smith, L. C., Ryan, J. C., Pitcher, L. H., & Pavelsky, T. M. (2019). Arctic-Boreal lake dynamics revealed using CubeSat imagery. *Geophysical Research Letters*. https://doi.org/10.1029/2018GL081584

Dahl, T. E. (2011). *Status and trends of wetlands in the conterminous United States 2004 to 2009* (p. 108). U.S. Department of the Interior; Fish and Wildlife Service.

DelSontro, T., Beaulieu, J. J., & Downing, J. A. (2018). Greenhouse gas emissions from lakes and impoundments: Upscaling in the face of global change: GHG emissions from lakes and impoundments. *Limnology and Oceanography Letters*. https://doi.org/10.1002/lol2.10073

DeVries, B., Huang, C., Lang, M., Jones, J., Huang, W., Creed, I., & Carroll, M. (2017). Automated Quantification of Surface Water Inundation in Wetlands Using Optical Satellite Imagery. *Remote Sensing*, *9*(8), 807. https://doi.org/10.3390/rs9080807

Downing, J. A., Prairie, Y. T., Cole, J. J., Duarte, C. M., Tranvik, L. J., Striegl, R. G., McDowell, W. H., Kortelainen, P., Caraco, N. F., Melack, J. M., & Middelburg, J. J. (2006). The global abundance and size distribution of lakes, ponds, and impoundments. *Limnology and Oceanography*, *51*(5), 2388–2397. https://doi.org/10.4319/lo.2006.51.5.2388

Evenson, G. R., Golden, H. E., Lane, C. R., McLaughlin, D. L., & D'Amico, E. (2018). Depressional wetlands affect watershed hydrological, biogeochemical, and ecological functions. *Ecological Applications*, *28*(4), 953–966. https://doi.org/10.1002/eap.1701

Evenson, G. R., McLaughlin, D. L., Lane, C. R., DeVries, B., Alexander, L. C., Lang, M. W., McCarty, G. W., & Sharifi, A. (2018). A watershed-scale model for depressional wetland-rich landscapes. *Journal of Hydrology X*, *1*, 100002. https://doi.org/10.1016/j.hydroa.2018.10.002

Fenstermacher, D. E., Rabenhorst, M. C., Lang, M. W., McCarty, G. W., & Needelman, B. A. (2014). Distribution, Morphometry, and Land Use of Delmarva Bays. *Wetlands*, *34*(6), 1219–1228. https://doi.org/10.1007/s13157-014-0583-5

Fisher, T., Jordan, T., Staver, K., Gustafson, A., Koskelo, A., Fox, R., Sutton, A., Kana, T., Beckert, K., Stone, J., McCarty, G., & Lang, M. (2010). The Choptank Basin in Transition: Intensifying Agriculture, Slow

Urbanization, and Estuarine Eutrophication. In M. Kennish & H. Paerl (Eds.), *Coastal Lagoons* (Vol. 20103358, pp. 135–165). CRC Press. https://doi.org/10.1201/EBK1420088304-c7

Griffin, C. G., McClelland, J. W., Frey, K. E., Fiske, G., & Holmes, R. M. (2018). Quantifying CDOM and DOC in major Arctic rivers during ice-free conditions using Landsat TM and ETM+ data. *Remote Sensing of Environment*, *209*, 395–409. https://doi.org/10.1016/j.rse.2018.02.060

Grinham, A., Albert, S., Deering, N., Dunbabin, M., Bastviken, D., Sherman, B., Lovelock, C. E., & Evans, C. D. (2018). The importance of small artificial water bodies as sources of methane emissions in Queensland, Australia. *Hydrology and Earth System Sciences*, *22*(10), 5281–5298. https://doi.org/10.5194/hess-22-5281-2018

Halabisky, M., Moskal, L. M., Gillespie, A., & Hannam, M. (2016). Reconstructing semi-arid wetland surface water dynamics through spectral mixture analysis of a time series of Landsat satellite images (1984–2011). *Remote Sensing of Environment*, *177*, 171–183. https://doi.org/10.1016/j.rse.2016.02.040

Hanson, P. C., Carpenter, S. R., Cardille, J. A., Coe, M. T., & Winslow, L. A. (2007). Small lakes dominate a random sample of regional lake characteristics. *Freshwater Biology*, *52*(5), 814–822. https://doi.org/10.1111/j.1365-2427.2007.01730.x

Holgerson, M. A., & Raymond, P. A. (2016). Large contribution to inland water CO2 and CH4 emissions from very small ponds. *Nature Geoscience*, *9*(3), 222–226. https://doi.org/10.1038/ngeo2654

Hosen, J. D., Armstrong, A. W., & Palmer, M. A. (2018). Dissolved organic matter variations in coastal plain wetland watersheds: The integrated role of hydrological connectivity, land use, and seasonality. *Hydrological Processes*, *32*(11), 1664–1681. https://doi.org/10.1002/hyp.11519

Huang, C., Peng, Y., Lang, M., Yeo, I.-Y., & McCarty, G. (2014). Wetland inundation mapping and change monitoring using Landsat and airborne LiDAR data. *Remote Sensing of Environment*, *141*, 231–242. https://doi.org/10.1016/j.rse.2013.10.020

Ji, L., Zhang, L., & Wylie, B. (2009). Analysis of Dynamic Thresholds for the Normalized Difference Water Index. *Photogrammetric Engineering & Remote Sensing*, *75*(11), 1307–1317. https://doi.org/10.14358/PERS.75.11.1307

Jia, K., Jiang, W., Li, J., & Tang, Z. (2018). Spectral matching based on discrete particle swarm optimization: A new method for terrestrial water body extraction using multi-temporal Landsat 8 images. *Remote Sensing of Environment, 209*, 1–18. https://doi.org/10.1016/j.rse.2018.02.012

Jin, S., Homer, C., Yang, L., Danielson, P., Dewitz, J., Li, C., Zhu, Z., Xian, G., & Howard, D. (2019). Overall Methodology Design for the United States National Land Cover Database 2016 Products. *Remote Sensing, 11*(24), 2971. https://doi.org/10.3390/rs11242971

Jones, C. N., Evenson, G. R., McLaughlin, D. L., Vanderhoof, M. K., Lang, M. W., McCarty, G. W., Golden, H. E., Lane, C. R., & Alexander, L. C. (2018). Estimating restorable wetland water storage at landscape scales. *Hydrological Processes, 32*(2), 305–313. https://doi.org/10.1002/hyp.11405

Kuhn, C., de Matos Valerio, A., Ward, N., Loken, L., Sawakuchi, H. O., Kampel, M., Richey, J., Stadler, P., Crawford, J., Striegl, R., Vermote, E., Pahlevan, N., & Butman, D. (2019). Performance of Landsat-8 and Sentinel-2 surface reflectance products for river remote sensing retrievals of chlorophyll-a and turbidity. *Remote Sensing of Environment, 224*, 104–118. https://doi.org/10.1016/j.rse.2019.01.023

Lang, M. W., & Kasischke, E. S. (2008). Using C-Band Synthetic Aperture Radar Data to Monitor Forested Wetland Hydrology in Maryland's Coastal Plain, USA. *IEEE Transactions on Geoscience and Remote Sensing, 46*(2), 535–546. https://doi.org/10.1109/TGRS.2007.909950

Lang, M. W., Kasischke, E. S., Prince, S. D., & Pittman, K. W. (2008). Assessment of C-band synthetic aperture radar data for mapping and monitoring Coastal Plain forested wetlands in the Mid-Atlantic Region, U.S.A. *Remote Sensing of Environment, 112*(11), 4120–4130. https://doi.org/10.1016/j.rse.2007.08.026

Lang, M. W., Kim, V., McCarty, G. W., Li, X., Yeo, I.-Y., Huang, C., & Du, L. (2020). Improved Detection of Inundation below the Forest Canopy using Normalized LiDAR Intensity Data. *Remote Sensing, 12*(4), 707. https://doi.org/10.3390/rs12040707

Lang, McDonough, O., McCarty, G., Oesterling, R., & Wilen, B. (2012). Enhanced Detection of Wetland-Stream Connectivity Using LiDAR. *Wetlands, 32*(3), 461–473. https://doi.org/10.1007/s13157-012-0279-7

Lee, McCarty, G. W., Moglen, G. E., Lang, M. W., Nathan Jones, C., Palmer, M., Yeo, I.-Y., Anderson, M., Sadeghi, A. M., & Rabenhorst, M. C. (2020). Seasonal drivers of geographically isolated wetland hydrology in a low-gradient, Coastal Plain landscape. *Journal of Hydrology, 583*, 124608. https://doi.org/10.1016/j.jhydrol.2020.124608

Lee, Yeo, I.-Y., Lang, M. W., McCarty, G. W., Sadeghi, A. M., Sharifi, A., Jin, H., & Liu, Y. (2019). Improving the catchment scale wetland modeling using remotely sensed data. *Environmental Modelling & Software*, *122*, 104069. https://doi.org/10.1016/j.envsoft.2017.11.001

Lindsay, J. B. (2016). Whitebox GAT: A case study in geomorphometric analysis. *Computers & Geosciences*, *95*, 75–84. https://doi.org/10.1016/j.cageo.2016.07.003

Lowe, W. H., & Likens, G. E. (2005). Moving Headwater Streams to the Head of the Class. *BioScience*, *55*(3), 196. https://doi.org/10.1641/0006-3568(2005)055[0196:MHSTTH]2.0.CO;2

McFeeters, S. K. (1996). The use of the Normalized Difference Water Index (NDWI) in the delineation of open water features. *International Journal of Remote Sensing*, *17*(7), 1425–1432. https://doi.org/10.1080/01431169608948714

Melton, J. R., Wania, R., Hodson, E. L., Poulter, B., Ringeval, B., Spahni, R., Bohn, T., Avis, C. A., Beerling, D. J., Chen, G., Eliseev, A. V., Denisov, S. N., Hopcroft, P. O., Lettenmaier, D. P., Riley, W. J., Singarayer, J. S., Subin, Z. M., Tian, H., Zürcher, S., … Kaplan, J. O. (2013). Present state of global wetland extent and wetland methane modelling: Conclusions from a model inter-comparison project (WETCHIMP). *Biogeosciences*, *10*(2), 753–788. https://doi.org/10.5194/bg-10-753-2013

Ollivier, Q. R., Maher, D. T., Pitfield, C., & Macreadie, P. I. (2019). Punching above their weight: Large release of greenhouse gases from small agricultural dams. *Global Change Biology*, *25*(2), 721–732. https://doi.org/10.1111/gcb.14477

Pangala, S. R., Enrich-Prast, A., Basso, L. S., Peixoto, R. B., Bastviken, D., Hornibrook, E. R. C., Gatti, L. V., Ribeiro, H., Calazans, L. S. B., Sakuragui, C. M., Bastos, W. R., Malm, O., Gloor, E., Miller, J. B., & Gauci, V. (2017). Large emissions from floodplain trees close the Amazon methane budget. *Nature*. https://doi.org/10.1038/nature24639

Parker, R. J., Boesch, H., McNorton, J., Comyn-Platt, E., Gloor, M., Wilson, C., Chipperfield, M. P., Hayman, G. D., & Bloom, A. A. (2018). Evaluating year-to-year anomalies in tropical wetland methane emissions using satellite CH4 observations. *Remote Sensing of Environment*, *211*, 261–275. https://doi.org/10.1016/j.rse.2018.02.011

Pekel, J.-F., Cottam, A., Gorelick, N., & Belward, A. S. (2016). High-resolution mapping of global surface water and its long-term changes. *Nature*, *540*(7633), 418–422. https://doi.org/10.1038/nature20584

Phillips, P. J., & Shedlock, R. J. (1993). Hydrology and chemistry of groundwater and seasonal ponds in the Atlantic Coastal Plain in Delaware, USA. *Journal of Hydrology*, *141*(1–4), 157–178. https://doi.org/10.1016/0022-1694(93)90048-E

Planet. (2018). *Planet Imagery Product Specification: Planetscope and RapidEye*. https://www.planet.com/products/satellite-imagery/files/Planet_Combined_Imagery_Product_Specs_December2017.pdf

Poulter, B., Bousquet, P., Canadell, J. G., Ciais, P., Peregon, A., Saunois, M., Arora, V. K., Beerling, D. J., Brovkin, V., Jones, C. D., Joos, F., Gedney, N., Ito, A., Kleinen, T., Koven, C. D., McDonald, K., Melton, J. R., Peng, C., Peng, S., … Zhu, Q. (2017). Global wetland contribution to 2000–2012 atmospheric methane growth rate dynamics. *Environmental Research Letters*, *12*(9), 094013. https://doi.org/10.1088/1748-9326/aa8391

Raymond, P. A., Hartmann, J., Lauerwald, R., Sobek, S., McDonald, C., Hoover, M., Butman, D., Striegl, R., Mayorga, E., Humborg, C., Kortelainen, P., Dürr, H., Meybeck, M., Ciais, P., & Guth, P. (2013). Global carbon dioxide emissions from inland waters. *Nature*, *503*(7476), 355–359. https://doi.org/10.1038/nature12760

Saunois, M., Stavert, A. R., Poulter, B., Bousquet, P., Canadell, J. G., Jackson, R. B., Raymond, P. A., Dlugokencky, E. J., Houweling, S., Patra, P. K., Ciais, P., Arora, V. K., Bastviken, D., Bergamaschi, P., Blake, D. R., Brailsford, G., Bruhwiler, L., Carlson, K. M., Carrol, M., … Zhuang, Q. (2020). The Global Methane Budget 2000–2017. *Earth System Science Data*, *12*(3), 1561–1623. https://doi.org/10.5194/essd-12-1561-2020

Seekell, D. A., Carr, J. A., Gudasz, C., & Karlsson, J. (2014). Upscaling carbon dioxide emissions from lakes: Upscaling CO2 emissions from lakes. *Geophysical Research Letters*, *41*(21), 7555–7559. https://doi.org/10.1002/2014GL061824

Stanley, E. H., Casson, N. J., Christel, S. T., Crawford, J. T., Loken, L. C., & Oliver, S. K. (2015). The ecology of methane in streams and rivers: Patterns, controls, and global significance. *Ecological Monographs*. https://doi.org/10.1890/15-1027.1

505 Thornton, B. F., Wik, M., & Crill, P. M. (2016). Double-counting challenges the accuracy of high-latitude methane
506 inventories: DOUBLE-COUNTING ARCTIC METHANE. *Geophysical Research Letters*, *43*(24), 12,569-
507 12,577. https://doi.org/10.1002/2016GL071772
508 Tranvik, L. J., Downing, J. A., Cotner, J. B., Loiselle, S. A., Striegl, R. G., Ballatore, T. J., Dillon, P., Finlay, K.,
509 Fortino, K., Knoll, L. B., Kortelainen, P. L., Kutser, T., Larsen, Soren., Laurion, I., Leech, D. M.,
510 McCallister, S. L., McKnight, D. M., Melack, J. M., Overholt, E., … Weyhenmeyer, G. A. (2009). Lakes
511 and reservoirs as regulators of carbon cycling and climate. *Limnology and Oceanography*, *54*(6part2),
512 2298–2314. https://doi.org/10.4319/lo.2009.54.6_part_2.2298
513 Treat, C. C., Bloom, A. A., & Marushchak, M. E. (2018). Non-growing season methane emissions are a significant
514 component of annual emissions across northern ecosystems. *Global Change Biology*.
515 https://doi.org/10.1111/gcb.14137
516 Tucker, C. J. (1979). Red and photographic infrared linear combinations for monitoring vegetation. *Remote Sensing*
517 *of Environment*, *8*(2), 127–150. https://doi.org/10.1016/0034-4257(79)90013-0
518 U. S. Fish and Wildlife Service. (2019). *National Wetlands Inventory website*. U.S. Department of the Interior, Fish
519 and Wildlife Service. http://www.fws.gov/wetlands/
520 Vanderhoof, M. K., Distler, H. E., Lang, M. W., & Alexander, L. C. (2018). The influence of data characteristics on
521 detecting wetland/stream surface-water connections in the Delmarva Peninsula, Maryland and Delaware.
522 *Wetlands Ecology and Management*, *26*(1), 63–86. https://doi.org/10.1007/s11273-017-9554-y
523 Vanderhoof, M. K., & Lang, M. (2017). *Data Release for the influence of data characteristics on detecting*
524 *wetland/stream surface-water connections in the Delmarva Peninsula, Maryland and Delaware* [Data set].
525 U.S. Geological Survey. https://doi.org/10.5066/F70C4T8F
526 Vermote, E. F., Tanre, D., Deuze, J. L., Herman, M., & Morcette, J.-J. (1997). Second Simulation of the Satellite
527 Signal in the Solar Spectrum, 6S: An overview. *IEEE Transactions on Geoscience and Remote Sensing*,
528 *35*(3), 675–686. https://doi.org/10.1109/36.581987
529 Wania, R., Melton, J. R., Hodson, E. L., Poulter, B., Ringeval, B., Spahni, R., Bohn, T., Avis, C. A., Chen, G.,
530 Eliseev, A. V., Hopcroft, P. O., Riley, W. J., Subin, Z. M., Tian, H., Brovkin, V., van Bodegom, P. M.,
531 Kleinen, T., Yu, Z. C., Singarayer, J. S., … Kaplan, J. O. (2012). Present state of global wetland extent and
532 wetland methane modelling: Methodology of a model intercomparison project (WETCHIMP).

Geoscientific Model Development Discussions, *5*(4), 4071–4136. https://doi.org/10.5194/gmdd-5-4071-2012

Winslow, L. A., Zwart, J. A., Batt, R. D., Dugan, H. A., Woolway, R. I., Corman, J. R., Hanson, P. C., & Read, J. S. (2016). LakeMetabolizer: An R package for estimating lake metabolism from free-water oxygen using diverse statistical models. *Inland Waters*, *6*(4), 622–636. https://doi.org/10.1080/IW-6.4.883

Wu, Q., Lane, C., & Liu, H. (2014). An Effective Method for Detecting Potential Woodland Vernal Pools Using High-Resolution LiDAR Data and Aerial Imagery. *Remote Sensing*, *6*(11), 11444–11467. https://doi.org/10.3390/rs61111444

Xaypraseuth, P., Satish, R., & Chatterjee, A. (2015). NISAR spacecraft concept overview: Design challenges for a proposed flagship dual-frequency SAR mission. *2015 IEEE Aerospace Conference*, 1–11. https://doi.org/10.1109/AERO.2015.7118935

Yeo, I.-Y., Lang, M. W., Lee, S., McCarty, G. W., Sadeghi, A. M., Yetemen, O., & Huang, C. (2019). Mapping landscape-level hydrological connectivity of headwater wetlands to downstream waters: A geospatial modeling approach - Part 1. *Science of The Total Environment*, *653*, 1546–1556. https://doi.org/10.1016/j.scitotenv.2018.11.238

Zeileis, A., Fisher, J. C., Hornik, K., Ihaka, R., McWhite, C. D., Murrell, P., Stauffer, R., & Wilke, C. O. (2019). colorspace: A Toolbox for Manipulating and Assessing Colors and Palettes. *ArXiv:1903.06490 [Cs, Stat]*. http://arxiv.org/abs/1903.06490

Figure1.

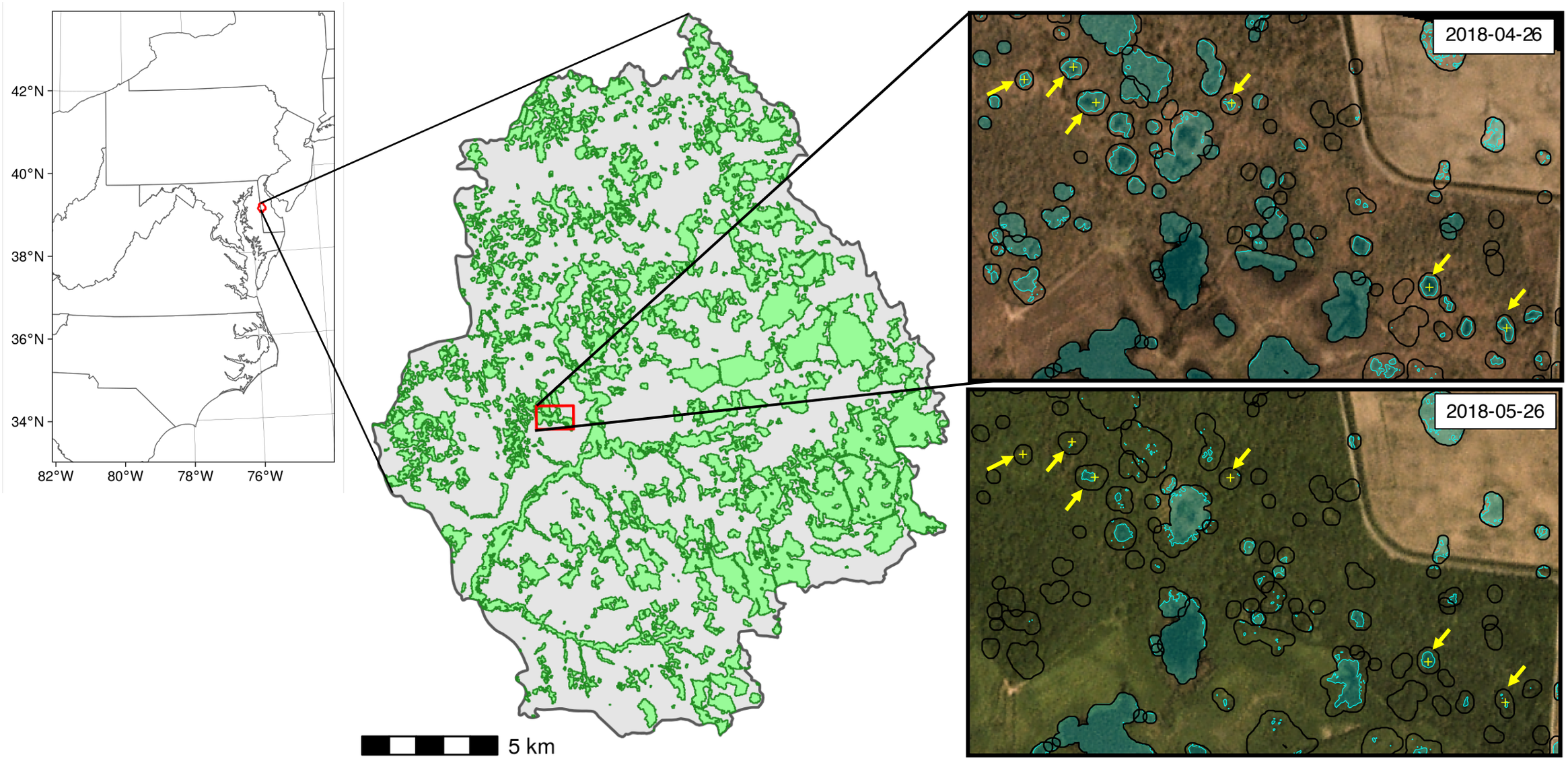
42°N
40°N
38°N
36°N
34°N
82°W
80°W
78°W
76°W
5 km
2018-04-26
2018-05-26

Figure2.

a) For each image

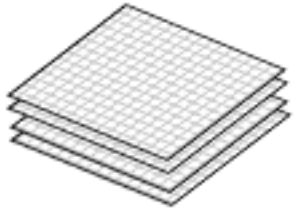

1. Calculate additional bands

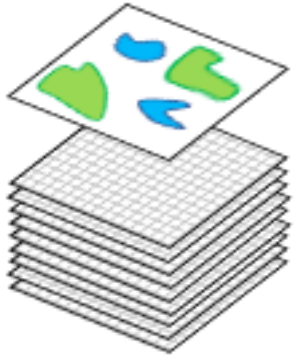

2. Train image-specific classification model

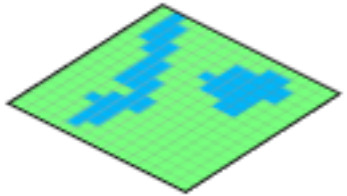

3. Apply model to predict inundation

b) For each wetland

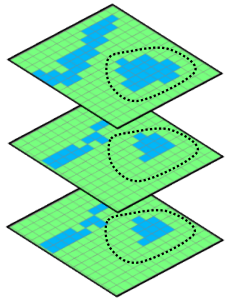

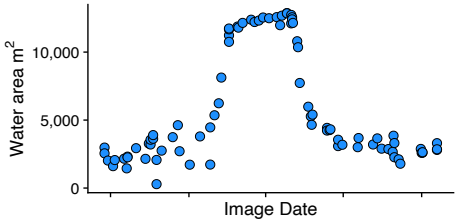

4. Sum water area within polygon for each image

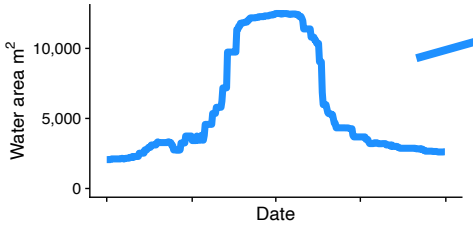

5. Calculate daily water area using moving average

c) Methane flux

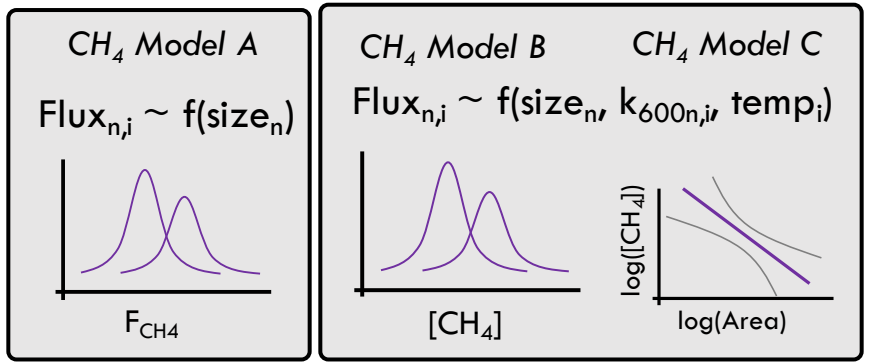

6. Sample daily wetland-specific areal flux rate from diffusive flux models

$$\text{Emissions} = \sum\sum (\mathbf{SWE}_{n,i}) \times (\mathbf{Flux}_{n,i})$$

7. Sum annual watershed emissions using daily surface water extent and flux rate time series for each wetland

Figure3.

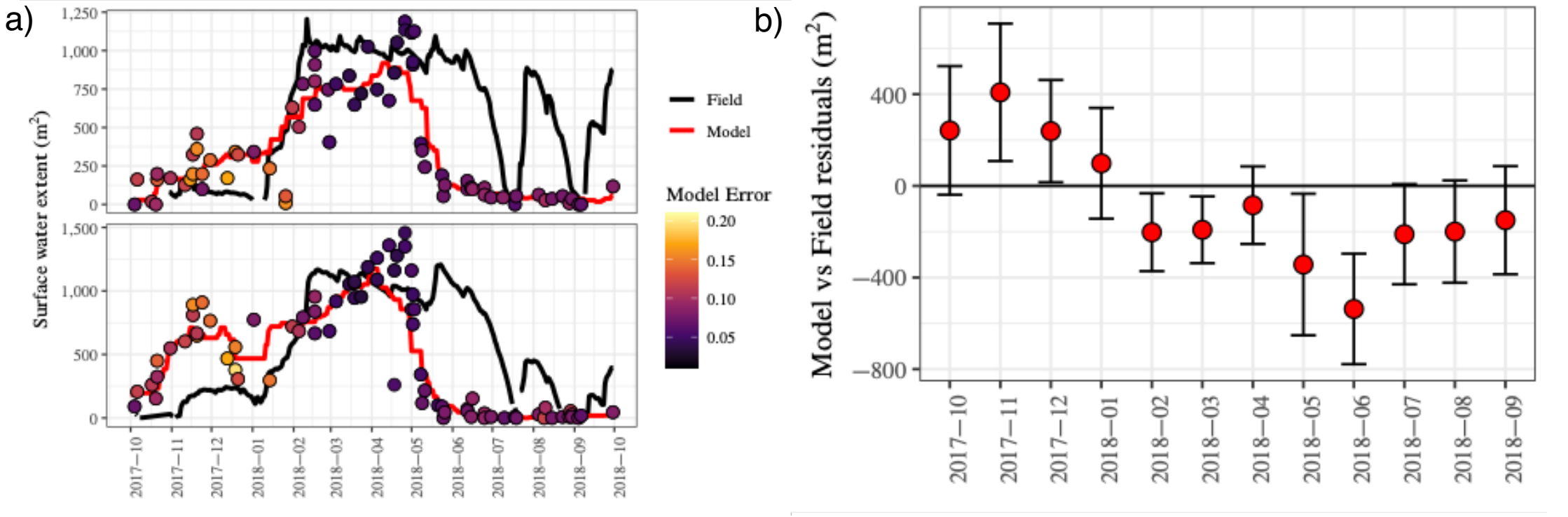
a)
Surface water extent (m²)
1,250
1,000
750
500
250
0
1,500
1,000
500
0
2017—10
2017—11
2017—12
2018—01
2018—02
2018—03
2018—04
2018—05
2018—06
2018—07
2018—08
2018—09
2018—10
Field
Model
Model Error
0.20
0.15
0.10
0.05
b)
Model vs Field residuals (m²)
400
0
−400
−800
2017—10
2017—11
2017—12
2018—01
2018—02
2018—03
2018—04
2018—05
2018—06
2018—07
2018—08
2018—09

Figure4.

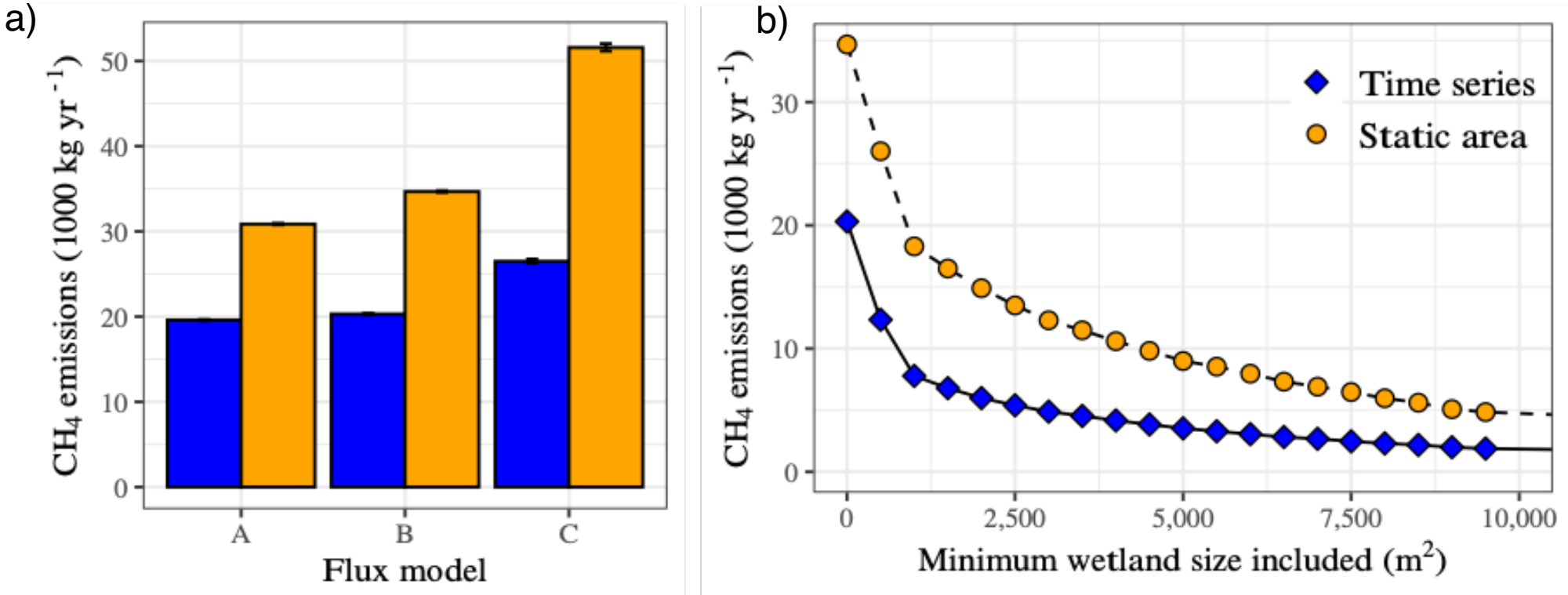
a)
CH_4 emissions (1000 kg yr^{-1})
0
10
20
30
40
50
A
B
C
Flux model
b)
CH_4 emissions (1000 kg yr^{-1})
0
10
20
30
Time series
Static area
0
2,500
5,000
7,500
10,000
Minimum wetland size included (m^2)